35th Annual International Conference of the IEEE EMBS
Osaka, Japan, 3 - 7 July, 2013

Automated Localization of Cysts in Diabetic Macular Edema using Optical Coherence Tomography Images

Sohini Roychowdhury[1], Dara D. Koozekanani[2], Salma Radwan[2] and Keshab K. Parhi[1]

Abstract— **This paper presents a novel automated system that localizes cysts in optical coherence tomography (OCT) images of patients with diabetic macular edema (DME). First, in each image, six sub-retinal layers are detected using an iterative high-pass filtering approach. Next, significantly dark regions within the retinal micro-structure are detected as candidate cystoid regions. Each candidate cystoid region is then further analyzed using solidity, mean and maximum pixel value of the negative OCT image as decisive features for estimating the area of cystoid regions. The proposed system achieves 90% correlation between the estimated cystoid area and the manually marked area, and a mean error of 4.6%. Finally the proposed algorithm locates the cysts in the inner plexiform region, inner nuclear region and outer nuclear region with an accuracy of 88%, 86% and 80%, respectively.**

Index Terms: Optical coherence tomography, diabetic macular edema, iterative segmentation, correlation coefficient, cystoid area

I. INTRODUCTION

Diabetic Macular Edema (DME) is the biggest cause of acquired blindness due to prolonged diabetes. The World Health Organization estimates that by the year 2020, there will be 75 million blind people and 314 million partially blind people in the world [1]. It is estimated that about 5% of this populations suffer from diabetic retinopathy. The goal of this paper is to develop a tool that can segment the OCT images to 6 sub-retinal layers, and can locate cysts in these layers. Such an automated cyst localization system can detect retinal pathologies and help in prioritizing eye-care delivery.

Optical Coherence Tomography (OCT) has been widely used to assess macular diseases, and it has enabled elaborate characterization of the cysts that develop in the sub-retinal layers due to DME. Studies have shown that the volume of retinal tissue within fluid-filled spaces in the retina can be an accurate predictor of visual acuity [2]. Further, clinical studies based on the volume of cystoid fluid and the location of the cysts may be used as a metric for visual prognosis. Motivated by this, we propose an automated system to detect cysts in OCT images from DME patients by estimating the area and location of the cystoid regions per image. These area estimates from adjacent OCT scans can then be combined to obtain cystoid volumes. Additionally, the presence of diabetic cysts may alter the normal pattern of the sub-retinal layers leading to sub-retinal *disorganization*. The extent of disorganization can be estimated using our method of localizing these cysts in certain sub-retinal layers.

[1]Department of Electrical and Computer Engineering, University of Minnesota, Minneapolis, MN 55455

[2]Department of Ophthalmology, University of Minnesota, Minneapolis, MN 55455

Several prior efforts for segmentation of sub-retinal layers have identified up to 9 sub-retinal layers in OCT images [3]. However, only one method has been reported so far for segmentation of cystoid volume [2]. This method identifies the regions of cystoid volume in 3-D stacks by bilateral filtering followed by thresholding and boundary tracing. In [2], cyst volume is estimated within 0-12% absolute error for OCT image stacks from 19 patients; however, this method suffers from under-estimation of cystic fluid volume. This drawback introduces false negatives while estimating diabetic cysts, which is undesired. Also, methods for detecting the location of cysts for estimating the extent of retinal disorganization have not yet been published.

This paper makes two key contributions. First, we present an algorithm that estimates the area of diabetic cysts within a certain region of interest (ROI). The correlation coefficient of the cystoid area between automated and manually traced area is 0.9. Additionally, our algorithm is capable of determining the boundaries of contiguous cysts by breaking down large cysts. The proposed system achieves an over detection of cystoid area with 4.6% mean and 6.6% standard deviation based on 120 OCT images of 25 DME patients. The second contribution is the automated localization of the diabetic cysts. Our algorithm segments the OCT images into six sub-retinal layers, followed by the detection of dark cystoid regions within the six sub-retinal layers. This enables localization of the cysts to particular inner and outer retinal regions. Our method achieves 100% sensitivity and 75% specificity in separating images with no cysts from the ones with cysts, and it achieves greater than 80% accuracy for detecting cysts in the inner and outer sub-retinal regions.

II. PROPOSED METHOD

OCT images generally suffer from speckle noise that may introduce false edges if not removed in the early stages of automated processing. So far, OCT speckle denoising has been accomplished using Wiener filtering [4] or Bayesian least-squares estimation [5]. In this work, we rely on median filtering [6] since it smoothens the sub-retinal layers while retaining the fine cyst boundaries. Next, the images are segmented to detect six sub-retinal layers by iterative high-pass filtering. This is followed by the detection of the cystoid regions that may appear in the sub-retinal micro-structure.

A. Problem Formulation

The green plane of each RGB image in JPEG format, that carries the most information, is first scaled in the range [0,1]. Then, the image is denoised by median filtering followed by

978-1-4577-0216-7/13/$26.00 ©2013 IEEE

extracting a particular square region of interest where each side is 1500 μm to generate the image Y shown in Fig. 1. In each image Y, regions corresponding to six sub-retinal layers (I_R) are detected by iterative high-pass filtering and thresholding. ROI is defined as the region between the first sub-retinal layer and the sixth layer. The area of this ROI (A) is useful in computing the extent of disorganization for visual prognosis.

Next, diabetic cysts are detected within the ROI as regions that are significantly darker than the immediate neighborhood. This process is further fine-tuned to improve the sensitivity and specificity. Finally, the area ($\hat{x}$) and location of the automatically detected cysts as shown in Fig. 1 are compared to the manually measured area (x) and sub-retinal locations for analyzing the accuracy of the proposed method.

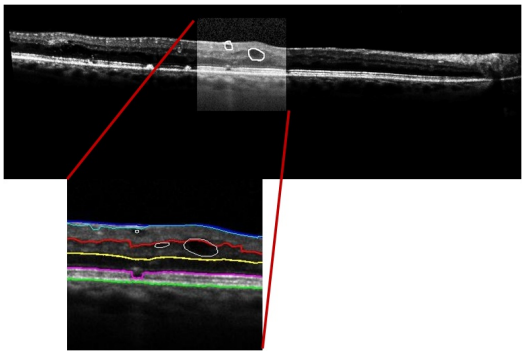

Fig. 1. OCT image with the square box corresponding to the region of interest is highlighted (Y) and manually annotated. The proposed automated system will segment the image into six sub-retinal layers (I_R). Area (A) of ROI is determined between the nerve fiber layer (blue) and the pigment epithelium (green). Finally the cysts are detected in particular sub-retinal layers (white).

B. Image Segmentation

Once the OCT images are denoised, 6 sub-retinal layers are segmented by iterative high-pass filtering in the spatial domain. Several segmentation methods such as edge detection followed by segment linking or gradient search methods are well established for automated segmentation for normal OCT images. Most such methods fail in the presence of sub-retinal cysts in OCT images with pathology [7] due to false interpolation, whereas our method does not need any interpolation, and thus detects retinal pathologies accurately.

We extract the sub-retinal layers by first estimating a mask of the region that contains the layer (Gm), and then high-pass filtering the image (Im) with the masked region of interest only as described by (1). Masking the image helps to concentrate attention to a certain region of the image at a time, thereby segmenting a complete region (I_R) in one iteration.

$$I_R = HPF(Im \circ Gm) \tag{1}$$
$$\Rightarrow I_R = Im \circ Gm - LPF(Im \circ Gm).$$

Here HPF and LPF represent the standard spatial high-pass filtered version and low-pass filtered version of the image, respectively, and $\circ$ represents per-element multiplication of matrices, or the Hadamard product.

To generate a mask for all the sub-retinal layers, the denoised and rescaled image (Y in [0,1]) is convolved with two double-Gaussian filters in the horizontal and vertical direction. The root mean squared resulting image followed by region-grow operation extracts a mask (G) for the region containing all the six sub-retinal layers. The upper boundary of G represents the retinal nerve fiber layer (NFL). We define a function $mask\ (top, bottom)$ that computes a mask for the region between the pixels mentioned as the top layer (top) and bottom layer ($bottom$).

Next, (1) is invoked repeatedly with $Gm = G, Im = Y$ and an averaging LPF to extract the region with highest solidity and area, such that its top layer represents the photoreceptor inner segment (PIS), while the bottom layer is the pigment epithelium (PE) as shown in Fig. 2. Then, the Hadamard product of $Gm = mask\ (NFL, PIS)$ with negative of the image ($Im = 1-Y$), and averaging LPF are used to extract the region with highest area whose bottom layer corresponds to the outer nuclear layer (ONL). This process is repeated with $Gm = mask\ (NFL, ONL)$ to extract the inner nuclear and outer plexiform layer (INL) similarly. Finally, $Gm = mask\ (NFL, INL)$ is combined with $Im = Y$ and a high-pass sobel filter is used to extract the inner plexiform layer and ganglion layer (IPL).

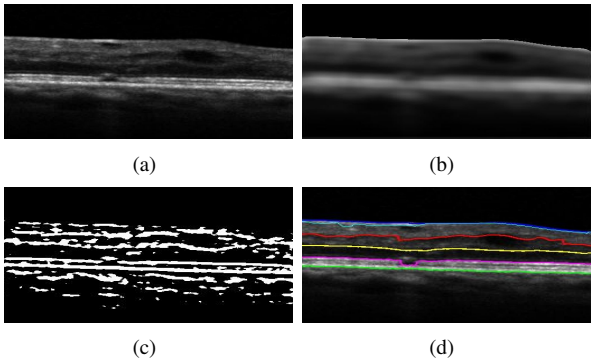

Fig. 2. Automated segmentation of 6 sub-retinal layers. (a) Original Image. (b) LPF version of denoised image. (c) HPF components detected after first iteration. (d) Final six layers color overlaid on original image as: NFL (Blue), IPL/GL (Cyan), INL (Red), ONL (Yellow), PIS (Magenta), PE (Green).

The six sub-retinal layers detected so far depict boundaries of certain regions within the retinal micro-structure with specific visual characteristics. Further, the extent of disorganization caused by diabetic cysts needs to be analyzed region wise. Hence, localization of cystoid regions is achieved for the inner plexiform region (IPR) between the IPL and the INL, the inner nuclear region (INR) between the INL and the ONL, and the outer nuclear region (ONR) between the ONL and the PIS.

C. Cyst Detection

After each image is segmented for sub-retinal layers, the next step is to detect diabetic cysts and fine-tune this

detection process to eliminate instances of false positives and false negatives. Cysts can be identified in a retinal micro structure as regions that are significantly darker than the immediate surrounding. Then the diabetic cysts in the IPR, INR and ONR are found using our proposed Algorithm 1 described below.

A mask is generated between the NFL and the PIS layer and the negative of the denoised image is globally thresholded using empirically determined thresholds to extract the possible cystoid regions (C_i). Next, the regions that are highly elliptical or that have large area are categorized as candidate large cysts (LC) while the others are candidate small cysts (SC). The LC regions are further enhanced in contrast and thresholded to generate candidate broken large cysts (BLC). Next, all BLCs and SCs are subjected to a cyst decision Algorithm 2, where the mean and maximum pixel value of the ONR in the negative image are compared with the mean and maximum pixel value of the candidate cystoid regions if the candidate cysts are in close vicinity of the ONR. If the candidate cystoid region pixel values significantly differ from the ONR pixel values, then the cystoid region is a true cyst (TC), else it is discarded as a false positive. The discriminating features for cysts, i.e., solidity, mean, and maximum pixel value of the negative image are selected after empirical experiments were conducted using shape and size features such as perimeter, axis lengths etc. Empirically determined thresholds $[\delta, t]$ are chosen as $[0.91, 0.05]$. Thus, the area of all the TCs ($\hat{x}$) and the location of these TCs are determined for analyzing the performance of the automated system compared to manual annotation.

1) Cyst Area Estimation: Our automated system detects candidate cystoid regions, and invokes the cyst decision algorithm to verify if a cystoid region is actually a cyst or a false positive that is highlighted because of a significantly dark ONR. This is depicted in Fig. 3.

2) Cyst Location Estimation: Once the six sub-retinal layers and the TCs are detected, masks corresponding to the IPR, INR and ONR are generated and the Hadamard product of these masks with the image containing the TC regions determines the location of the diabetic cysts as shown in Fig. 4.

III. RESULTS

We evaluate our automated cyst detection system using 120 images from 25 diabetic patients with DME. These images were acquired using the Heidelberg Spectralis imaging systems such that each image is obtained by averaging 12-19 frames with a resolution of 5.88μm/pixel along the length and 3.87μm/pixel along the width. The correlation (r) between the automated true cyst area ($\hat{x}$) and the manually marked cyst area (x) is estimated by the correlation coefficient given by (2).

$$r = \frac{\sum_{i=1}^{120}(x_i - \bar{x_i})(\hat{x_i} - \bar{\hat{x_i}})}{\sqrt{\sum_{i=1}^{120}(x_i - \bar{x_i})^2}\sqrt{\sum_{i=1}^{120}(\hat{x_i} - \bar{\hat{x_i}})^2}}. \quad (2)$$

Algorithm 1 Automated Cyst Detection (Y, NFL, PIS)

Require: $G_w \leftarrow mask(NFL, PIS)$
Require: $I_{cyst} \leftarrow \{enhance((1-Y) \circ G_w)\} > 0.7$
Require: $[mean_o, max_o] \leftarrow$ mean and maximum pixel value of the ONR
Let C_i represents all regions in $I_{cyst} \forall i = 1, 2, ...$
Let Small Cysts (SC)= $\{\}$, Large Cysts (LC)= $\{\}$, Broken Large Cysts (BLC)= $\{\}$, $\hat{x} = 0$, True Cysts (TC)= $\{\}$
Step 1: $\forall C_i$
if $\frac{major\ axis\ length(C_i)}{minor\ axis\ length(C_i)} < 7$ and $area(C_i) < 2000$ **then**
  $SC \leftarrow C_i$
else
  $LC \leftarrow C_i$
end if
Step 2: $\forall SC(j)$
D(j) $\leftarrow$ cyst decision($SC(j), mean_o, max_o$)
if D(j)=1 **then**
  TC $\leftarrow$ SC(j)
  $\hat{x} = \hat{x} + area(SC(j))$
end if
Step 3: $\forall LC(k)$
$BLC(l) \leftarrow \{enhance((1-Y) \circ LC(k))\} > 0.8$
Step 4: $\forall BLC(l)$
$D(l) \leftarrow$ cyst decision($BLC(l), mean_o, max_o$)
if D(l)=1 **then**
  TC $\leftarrow BLC(l)$
  $\hat{x} = \hat{x} + area(BLC(l))$
end if
return $\hat{x}$, TC

Algorithm 2 cyst decision ($S, mean_o, max_o$)

Require: $Solidity(S) = \frac{Area(S)}{Convex\ Area(S)}$
Require: $[mean_s, max_s] \leftarrow$ mean and maximum pixel value of the region in S
Let dist $\leftarrow$ shortest distance between centroid of S and the ONL
if dist < 10 **then**
  if $Solidity(S) > \delta$ **then**
    $D = 1$
  else
    if $abs(mean_s * max_s - mean_o * max_o) > t$ **then**
      $D = 1$
    else
      $D = 0$
    end if
  end if
else
  $D = 1$
end if
return D

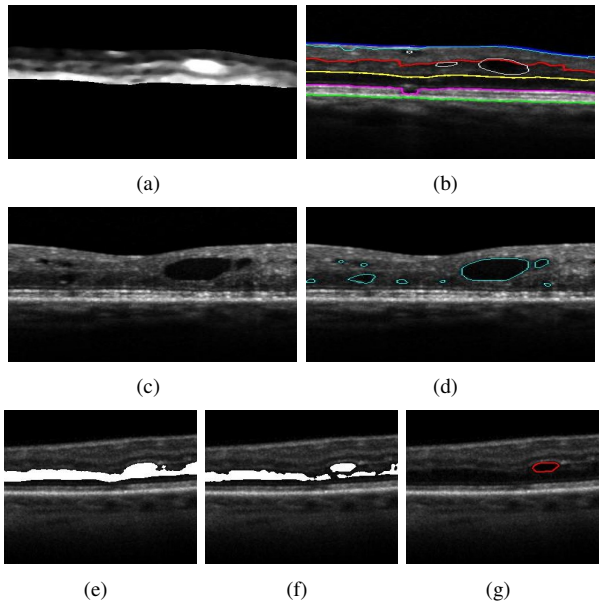

Fig. 3. Cyst detection. (a) Candidate cystoid regions after contrast enhancement appear brighter than the immediate neighborhood in the negative of the image within the NFL and PIS layers. (b) True cysts detected. (c) Actual image (d) True small cysts detected (e) Large cyst detected (f) Broken large cysts (g)True cysts detected after cyst decision algorithm is invoked.

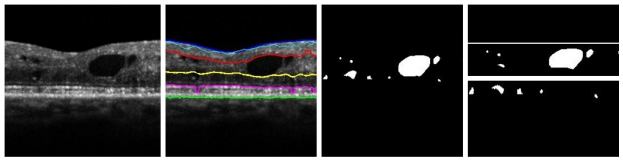

Fig. 4. The actual image is segmented and the region corresponding to the true cysts are combined with the segmented regions to determine the regions where the cysts appear. The right-most image represents the appearance of cysts in the IPR, INR and ONR from top to bottom.

We observe $r = 0.9$, which signifies a high correlation between manual and automated cyst area. Further analysis of the automated cyst area compared to the manual annotations is presented in Table I and illustrated in Fig. 5.

TABLE I

AUTOMATED DETECTION OF CYST AREA

Statistic	$\frac{x}{\hat{x}}$	True area (%) $\frac{x}{A} * 100$	Detected area (%) $\frac{\hat{x}}{A} * 100$	Abs area diff (%)
Mean	0.8504	11.43	14.30	4.61
Std. dev	0.3872	13.70	16.62	6.64

Next, automated localization of the cystoid regions as compared to manual localization is presented in Table II.

IV. CONCLUSIONS

This paper has proposed an automated diabetic cyst localization system using OCT images of patients with DME. The automated area of cysts detected is highly correlated

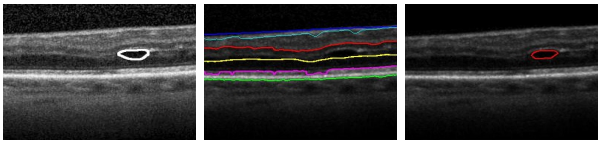

Fig. 5. Comparison of automated cyst detection system to manual markings. (a) Original image with cystoid region manually marked (b) Automated segmentation. Area of ROI (A) is the region between the NFL (blue) and the PE (green) layer. (c) Automated detection of cystoid region.

TABLE II

PERFORMANCE OF AUTOMATED CYST LOCALIZATION (%)

Task	SEN	SPEC	PPV	NPV	Acc
Separating images with/without cyst	100	75	91.67	100	93.33
Locating cysts in the IPR	91.3	83.33	88.73	86.96	88.03
Locating cysts in the INR	98.51	70.0	81.48	97.22	86.32
Locating cysts in the ONR	90.79	60.98	81.18	78.13	80.34

with the manually marked cysts ($r = 0.9$) and the proposed system over estimates cystoid area such that the mean ratio between the actual cyst area and detected area is 0.85. Also, our system results in a mean error of 4.6% in estimating the percentage of the area within the region of interest occupied by cysts as compared to existing works that report upto 12% mean error in cystoid estimation [2]. Finally, our system can detect cysts in the inner plexiform, inner nuclear and outer nuclear regions with accuracy of 88%, 86% and 80%, respectively. Future efforts will be directed towards analysis of additional OCT image stacks and automated estimation of the volume of cystoids from other imaging systems apart from the Spectralis. The proposed automated system can aid clinical studies aimed at monitoring visual prognosis and disease progression.

REFERENCES

[1] W. H. Organization, "Vision 2020 action plan for 2006 to 2011 planning meeting." Geneva. 11 July 2006.

[2] G. Wilkins, O. Houghton, and A. Oldenburg, "Automated segmentation of intraretinal cystoid fluid in optical coherence tomography," *IEEE Transactions on Biomedical Engineering*, vol. 59, no. 4, pp. 1109 – 1114, April 2012.

[3] L. Zhao, A. E. Elsner, C. A. Clark, T. Y. Chui, J. A. Papay, B. P. Haggerty, D. A. VanNasdale, and S. A. Burns, "Semi-automatic OCT segmentation of nine retinal layers," *ARVO*, no. 4092/D1180, 2012.

[4] Y. Liu, Y. Liang, G. Mu, and X. Zhu, "Deconvolution methods for image deblurring in optical coherence tomography," *J. Opt. Soc. Am. A*, vol. 26, no. 1, pp. 72–77, Jan 2009.

[5] A. Wong, A. Mishra, K. Bizheva, and D. A. Clausi, "General bayesian estimation for speckle noise reduction in optical coherence tomography retinal imagery," *Opt. Express*, vol. 18, no. 8, pp. 8338–8352, April 2010.

[6] J. Rogowska and M. E. Brezinski, "Image processing techniques for noise removal, enhancement and segmentation of cartilage OCT images," *Phys. Med. Biol.*, vol. 47, no. 4, pp. 641–655, 2002.

[7] J. Tokayer, A. Ortega, and D. Huang, "Sparsity-based retinal layer segmentation of optical coherence tomography images," pp. 449–452, 2011.